

---

# Simulated Adversarial Testing of Face Recognition Models

---

**Nataniel Ruiz**  
Boston University  
nruiz9@bu.edu

**Adam Kortylewski**  
Johns Hopkins University  
akortyl1@jhu.edu

**Weichao Qiu**  
Huawei  
qiuwch@gmail.com

**Cihang Xie**  
UC Santa Cruz  
cixie@ucsc.edu

**Sarah Adel Bargal**  
Boston University  
sbargal@bu.edu

**Alan Yuille\***  
Johns Hopkins University  
ayuille1@jhu.edu

**Stan Sclaroff\***  
Boston University  
sclaroff@bu.edu

## Abstract

Most machine learning models are validated and tested on fixed datasets. This can give an incomplete picture of the capabilities and weaknesses of the model. Such weaknesses can be revealed at test time in the real world. The risks involved in such failures can be loss of profits, loss of time or even loss of life in certain critical applications. In order to alleviate this issue, simulators can be controlled in a fine-grained manner using interpretable parameters to explore the *semantic image manifold*. In this work, we propose a framework for learning how to test machine learning algorithms using simulators in an adversarial manner in order to find weaknesses in the model before deploying it in critical scenarios. We apply this model in a face recognition scenario. We are the first to show that weaknesses of models trained on real data can be discovered using simulated samples. Using our proposed method, we can find adversarial synthetic faces that fool contemporary face recognition models. This demonstrates the fact that these models have weaknesses that are not measured by commonly used validation datasets. We hypothesize that this type of adversarial examples are not isolated, but usually lie in connected components in the latent space of the simulator. We present a method to find these *adversarial regions* as opposed to the typical adversarial points found in the adversarial example literature.

## 1 Introduction

Evaluating a machine learning model can have many pitfalls. Ideally, we would like to know (1) when the model will fail (2) in which way it will fail and (3) how badly it will fail. In other words, we would like to be able to accurately estimate the model’s risk on the true test data distribution as well as know what specific factors induce the model to failure. We would like to know how these failures will manifest themselves. For example, whether a face verification model will generate a false-positive or false-negative error. And finally, when this failure happens, we would like to know how confident was the incorrect decision by the model. Testing models is no longer a purely academic endeavour [48], with many high profile bad societal consequences being revealed in recent years due to insufficient testing particularly with respect to racial and gender bias in face analysis systems [5, 14, 16].

These three desiderata are very hard to achieve in practice. There are major philosophical and theoretical obstacles to achieve perfect knowledge of model failures a priori. Nevertheless, partial

---

\*Equal senior contribution.

knowledge of model weaknesses and predictions of model failures are possible. Yet, there are still major hurdles that stand in our way.

One such hurdle is the fact that *testing data is limited*, due to the fact that it is expensive to gather and label. It is not uncommon for a model to perform well on an assigned test set and fail to generalize to specific obscure examples when it is deployed. A second important hurdle is the fact that *testing data is unruly*. There are latent factors that generate the testing data, which are hard to control or even to fully understand. For example, a known factor that is hard to control is the lighting of a scene. Most datasets have been captured without controlling for this variable, and thus present an insufficient amount of variability in this respect. Testing a model in one environment could yield perfect performance, yet fail on an environment with more lighting variability. Even if a test dataset with carefully controlled lighting were assembled, the dataset would be very expensive and time-consuming to collect and there is no guarantee that the full variability would be explored.

A way to tackle these problems is to use simulators to generate test data. Such an approach can cheaply generate a large quantity of data spanning a large spectrum. Also, simulators are fully controllable and the generative parameters are known. This allows for careful exploration of situations where models fail. This includes the possibility to find interpretable factors that generate failures, to study the way these failures manifest themselves (is the model classifying a cat as a jaguar when there is green in the background?) and to examine the degrees of certainty of the model in these failure modes.

When simulating test data, we have full control over simulator parameters. Thus, we are able to explore the manifold generated by the simulator in the space of the simulator parameters. We call this manifold the *semantic image manifold*, in contrast to the *adversarial image manifold* that is explored in the traditional adversarial attack literature. A random exploration of this manifold is both inefficient and not the most informative approach. In this work we propose to ***test machine learning models using simulation in an adversarial manner*** by finding simulator parameters that generate samples that fool the model. We are inspired by the literature on adversarial examples that fool machine learning models, yet in contrast to this body of work, the adversarial examples that our simulator generates are *semantically realistic* in the sense that we are not adding low magnitude noise to an image in order to fool the model but finding semantically sensible image configurations that generate model failure. In this way, we are not investigating the well-known weakness of gradient-based models to unrealistic targeted noise but to plausible scenes that might be rare, yet mislead the model. We present a method that finds adversarial samples efficiently using a continuous policy that searches the high-dimensional space of possibilities.

A limitation of this type of work is that, in general there exists domain shift between the distribution described by the simulator and the real world distribution [13, 7, 43, 42, 17, 32]. Nevertheless, in our work we are able to show that in some situations, real model weaknesses can be found using simulated data. This gives credence to the hypothesis that, even though there is domain shift, simulated samples can be informative. Also, simulators are rapidly improving in terms of realism [37, 29, 10, 24]. This allows for greater opportunities to use these ideas in the future as simulated and real data distributions become more and more aligned.

Following our *semantic image manifold* hypothesis we conjecture that these adversarial examples are not isolated points in space, but instead are regions of this manifold. In prior work on traditional adversarial examples, optimization procedures find adversarial samples that are points in image space [41, 30, 6, 15, 27, 38]. In contrast to this body of work we propose a method to find these *adversarial regions* instead. This is valuable because ideally we would like to be able to fully describe the machine learning model’s *regions of reliability*, where model predictions will tend to be correct. With this knowledge a user would be able to avoid performing inference on a model outside of its scope in order to minimize failures.

Contributions of this work are three-fold. We summarize them as follows:

- We show that weaknesses of models trained on real data can be discovered using simulated samples. We perform experiments on face recognition networks showing that we can diagnose the weakness of a model trained on biased data.
- We present a method to find adversarial simulated samples in the *semantic image manifold* by finding adversarial simulator parameters that generate such samples. We present experiments

on contemporary face recognition networks showing that we can efficiently find faces that are incorrectly recognized by the network.

- We present a method to find *regions* that are adversarial, in order to locate danger zones where a model’s predictions are more liable to be incorrect. This is in contrast to the adversarial attack literature that finds isolated adversarial points instead of regions.

## 2 A Framework for Simulated Adversarial Testing

Here we formalize adversarial testing using a simulator. We postulate some assumptions on the data generation process in the real and simulator world. Then we write the risks for a machine learning model and the mathematical formulation to find adversarial parameters that yield samples that fool machine learning models. We then strike some parallels between our scenario and the literature on learning across domains. Finally, we describe our proposed algorithm to find such adversarial simulator parameters and adversarial samples.

Let us assume the real world data  $(x, y)$  (where  $x$  is the data and  $y$  is the label) is generated by the distribution  $p(x, y|\psi)$  where  $\psi$  is a latent variable that causally controls the data generation process. For example,  $\psi$  includes the object type in the image and the angle of view of such an object, as well as all other parameters that generate the scene and image. The risk for a discriminative model  $f$  is:

$$\mathbb{E}_{\psi \sim a} [\mathbb{E}_{(x, y) \sim p(x, y|\psi)} [L(f(x), y)]], \quad (1)$$

where  $a$  is the distribution of  $\psi$  and  $L$  is the loss. We can search for  $\psi^*$  that maximizes this risk:

$$\max_{\psi \in A} [\mathbb{E}_{(x, y) \sim p(x, y|\psi)} [L(f(x), y)]] \quad (2)$$

where  $A$  is the set of all possible  $\psi$ . Let us assume that we have  $\psi = (\psi_u, \psi_k)$ , a decomposition of  $\psi$  into two latent variables  $\psi_u$  and  $\psi_k$ . Furthermore, let us assume that  $\psi_u$  controls for unknown features of the image, and  $\psi_k$  controls for known features of the image such as the camera pose, or the object position with respect to the camera. We can write the average risk as:

$$\mathbb{E}_{\psi_u \sim a} [\mathbb{E}_{\psi_k \sim b} [\mathbb{E}_{(x, y) \sim p(x, y|\psi_u, \psi_k)} [L(f(x), y)]]], \quad (3)$$

where  $b$  is the distribution of  $\psi_k$ . In most scenarios, we do not have access to the real data distribution  $p$  and cannot sample from it at will. Additionally, it is very difficult to control the known latent variable  $\psi_k$  when generating data, and we do not even know what factors are hidden in the variable  $\psi_u$ , much less how to control it. Using simulated data we are able to fully control the generative process.

A simulator samples data  $(x, y) \sim q(x, y|\rho)$ , where  $q$  is the simulated data distribution and we have complete knowledge over the latent variable  $\rho$ . We are able to search for adversarial examples and compute estimates of the mean and worst-case risks using this simulator. For example, the parameter  $\rho^*$  that maximizes the risk is written as follows:

$$\max_{\rho \in C} [\mathbb{E}_{(x, y) \sim q(x, y|\rho)} [L(f(x), y)]] \quad (4)$$

where  $C$  is the space of all possible  $\rho$ . We can find  $\hat{\rho}^*$  and estimate of  $\rho^*$  by sampling (albeit inefficiently). In our case we are working in a less restrictive scenario since we do not try to find the global maximum  $\rho^*$ , instead we try to find any  $\rho$  where  $\mathbb{E}_{(x, y) \sim q(x, y|\rho)} [L(f(x), y)]$  is above the misclassification threshold.

If we assume that the distributions  $p$  and  $q$  are similar enough we can use the knowledge gathered in simulation to understand the possibilities of failure in the real world. Essentially, this is a different kind of domain shift problem. In a traditional setting of transfer learning between domains, we are concerned about minimizing the risk on a target domain by training on a source domain. In the binary classification case, let us define a domain as a pair consisting of a distribution  $p$  on inputs  $\mathcal{X}$  and a labeling function  $g_p : \mathcal{X} \rightarrow [0, 1]$ . We consider the *real domain* and the *simulated domain* denoted by  $(p, g_p)$  and  $(q, g_q)$  respectively.

We also introduce a *hypothesis* that is a function  $h : \mathcal{X} \rightarrow \{0, 1\}$ . We can write the risk of this hypothesis on  $p$  as:

$$\epsilon_p(h, g_p) = \mathbb{E}_{x \sim p} [|h(x) - g_p(x)|] \quad (5)$$

In traditional domain adaptation from simulation to reality, we seek to learn on distribution  $q$  and generalize to distribution  $p$ . We want to find a hypothesis that minimizes the risk on the target real world distribution  $\epsilon_p(h, g_p)$  by training on samples from  $q$ .

In our setting, we do not train on synthetic samples. Instead we want to find a relationship between testing a hypothesis  $h$  on samples from distribution  $q$  and testing  $h$  on samples from  $p$ . There exist bound results for the risks  $\epsilon_p(h, g_p)$  and  $\epsilon_q(h, g_q)$  in the work of Ben-David *et al.* [4]:

$$\epsilon_p(h, g_p) < \epsilon_q(h, g_q) + d_1(q, p) + \min\{\mathbb{E}_p[|g_q(x) - g_p(x)|], \mathbb{E}_q[|g_q(x) - g_p(x)|]\}, \quad (6)$$

where  $d_1$  is the variation divergence. The second term of the right hand side quantifies the difference between distributions  $q$  and  $p$ , and the third term of the right hand side is the difference between the labeling functions across domains, which is expected to be small.

Since this bound characterizes the cross-domain generalization error and  $\epsilon_q(h, g_q)$  will usually be minimized by the learning algorithm, it is useful for studying transfer learning between domains. There are some differences in our scenario since for us  $h$  is a fixed function that has been trained on the target domain and we would like to talk about individual examples instead of overall risk over distributions. Also, the bound is proven for a binary classification problem, whereas our target scenario can be multi-class classification or regression.

Assume there exists a mapping  $\tau : C \rightarrow A$  (where  $A$  is the set of all possible  $\rho$ ), that maps the simulated latent variables to real latent variables  $\psi = \tau(\rho)$ . In order for adversarial examples in the simulator domain to be informative in the real domain, we want to have a simulator such that:

$$\mathbb{P}_{(x_s, y_s) \sim q(x_s, y_s | \rho), (x_r, y_r) \sim p(x_r, y_r | \tau(\rho))} [|L(x_s, y_s) - L(x_r, y_r)| < \epsilon] > \theta \quad (7)$$

where  $\epsilon$  is small and  $\theta \in [0, 1]$  is large. This way, high-loss examples found in the semantic image manifold using simulation have a high probability of transferring to the real world. Since the simulator and real domain are different, this is a moderately strong assumption. Nevertheless, we show cases where this assumption holds in our experimental evaluations in Section 4.3.

**Finding Adversarial Parameters** Our task is then to find  $\rho$  such that the loss over samples generated with this latent variable is over the misclassification threshold  $T$ . One of the main difficulties in searching for latent variables that fulfill this condition is that in general the simulator  $q$  is non-differentiable. Thus, we turn to black-box optimization methods to search for adversarial parameters. Specifically, we use policy gradients [45] in order to find such parameters.

We define a policy  $\pi_\omega$  parameterized by  $\omega$  that can sample simulator parameters  $\rho \sim \pi_\omega(\rho)$ . We train this policy to generate simulator parameters that generate samples that obtain high loss when fed to the machine learning model  $f$ . For this we define a reward  $R$  that is equal to the negative loss  $L$  and we want to find the parameters  $\omega$  that maximize  $J(\omega) = \mathbb{E}_{\rho \sim \pi_\omega} [R]$ . Following the REINFORCE rule we obtain gradients for updating  $\omega$  as

$$\nabla_\omega J(\omega) = \mathbb{E}_{\rho \sim \pi_\omega} [\nabla_\omega \log(\pi_\omega) R(\rho)] . \quad (8)$$

An unbiased, empirical estimate of the above quantity is

$$\mathcal{L}(\omega) = \frac{1}{K} \sum_{k=1}^K \nabla_\omega \log(\pi_\omega) \hat{A}_k , \quad (9)$$

where  $\hat{A}_k = R(\omega_k) - \beta$  is the advantage estimate,  $\beta$  is a baseline,  $K$  is the number of different parameters  $\rho$  sampled in one policy forward pass and  $R(\rho_k)$  designates the reward obtained by evaluating  $f$  on  $(x_k, y_k) \sim q(x_k, y_k | \rho_k)$ . We show all of the steps of our method in Algorithm 1 and we show an illustration of our method applied to the face verification scenario in Figure 1.

### 3 Finding Adversarial Regions

Here we describe our method to find adversarial regions. Once an adversarial simulator latent vector  $\rho_{\text{adv}} \in \mathbb{R}^n$  have been found using Algorithm 1 we define a graph  $G = (V, E)$ .  $V$  are the vertices of the graph, obtained by discretizing the space around the adversarial point in grid with spacing  $\nu$  between vertices. The edges  $E$  of the graph connect neighboring vectors, with each vector having

---

**Algorithm 1:** Our adversarial testing approach using policy gradients.

---

**Result:** adversarial simulator parameters  $\rho_k$  and adversarial sample  $x_k$

```

for iteration=1,2,... do
  Generate  $K$  simulator parameters  $\rho_k \sim \pi_\omega(\rho_k)$ ; Generate  $K$  samples
   $(x_k, y_k) \sim q(x_k, y_k | \rho_k)$ 
  Test the discriminative model and obtain  $K$  losses  $L(f(x_k), y_k)$ 
  if  $\exists k \in \{1, \dots, K\}; L(f(x_k), y_k) > T$  then
    Terminate and yield adversarial sample  $x_k$  and adversarial simulator parameters  $\rho_k$ 
  end
  Compute rewards  $R(\rho_k)$ 
  Compute the advantage estimate  $\hat{A}_k = R(\rho_k) - \beta$ 
  Update  $\omega$  via equation 9
end

```

---

$2n$  neighbors. We find the connected region of adversarial examples  $\mathcal{R}_{\text{adv}}$  that is seeded by  $\rho_{\text{adv}}$  by following Algorithm 2.

In essence, our method follows the general idea of an area flooding algorithm [25, 40] with two main differences. First, that we discretize a continuous space that is  $n$ -dimensional instead of working on binary 2-dimensional image, and second, that we check for sample membership of  $\mathcal{R}_{\text{adv}}$  by testing whether the model loss is higher than the adversarial threshold  $L(f(x), y) > T$ .

---

**Algorithm 2:** Finding connected regions of adversarial examples.

---

**Result:** connected region of adversarial examples  $\mathcal{R}_{\text{adv}}$

**Data:** seed adversarial simulator parameters  $\rho_{\text{adv}}$

$\mathcal{R}_{\text{adv}} = \{\rho_{\text{adv}}\}$

Initialize a stack  $\chi$ .

Push  $2n$  neighbors of  $\rho_{\text{adv}}$  to  $\chi$ .

```

for  $i=1,2,\dots$  do
  Pop  $\rho_i$  from  $\chi$ 
  Sample  $(x_i, y_i) \sim q(x_i, y_i | \rho_i)$ 
  Test the discriminative model and obtain loss  $L(f(x_k), y_k)$ 
  if  $L(f(x_k), y_k) > T$  then
     $\mathcal{R}_{\text{adv}} = \mathcal{R}_{\text{adv}} \cup \{\rho_i\}$ 
    Push all neighbors of  $\rho_i$  that have not been visited to  $\chi$ 
  end
end

```

---

## 4 Experimental Results

### 4.1 Controllable Face Simulation

We use the FLAME face model [23] as a controllable face simulator with the Basel texture model [31]. FLAME uses a linear shape space trained from 3,800 3D scans of human heads and combines this linear shape space with an articulated jaw, neck, and eyeballs, pose-dependent corrective blendshapes, and additional global expression blendshapes. In this way, using shape and texture components we can generate faces with different identities. The synthetic faces that are generated in our work are new and do not mimic any existing person’s features. By changing the pose and expression components we can add variability to these faces. Moreover, we have full control over the scene lighting and the head and camera pose and position. In order to render our scene we use the PyTorch3D rendering framework. We extract the corresponding shape, texture and expression components from the real faces of the CASIA WebFace dataset using DECA [9].

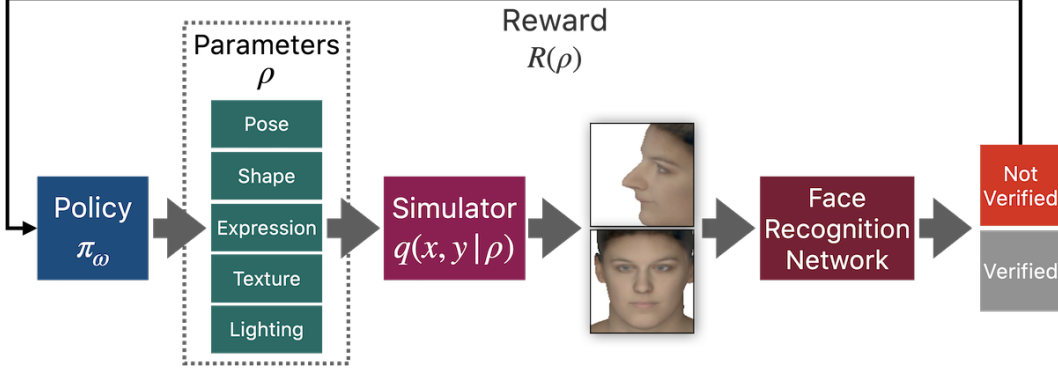


Figure 1: An illustration of our method applied to the face verification scenario. The simulator is conditioned on parameters that are generated by the policy. A pair of images of the same identity are generated. Face verification is run on this image pair using the face recognition network that is to be diagnosed. A reward is computed based on the correct or incorrect prediction of the network and the policy parameters are updated accordingly.

## 4.2 Models, Datasets and Infrastructure

In our experiments we use the CASIA WebFace [47] dataset for training the face recognition models and the LFW [18] dataset for real-world data testing. We use a Convolutional Block Attention Module (CBAM) [46] ResNet50 with CosFace [44] loss as the face recognition model. We use a multivariate Gaussian policy  $\pi(\rho) = \mathcal{N}(\mu_\pi, \sigma_\pi^2)$  where the variance is fixed  $\sigma_\pi^2 = 0.05 \times I$  and  $\mu_\pi$  is learned. We use a GeForce RTX 2080 GPU with 11GB of memory to perform all of our experiments. The policy, the face recognition network, the face model decoders and the renderer run on the same GPU.

## 4.3 Testing Weakened Models

We present a way to verify that knowledge from simulated weaknesses translates to real-world weaknesses. We weaken two networks by training on the CASIA WebFace dataset with images that exhibit a yaw parameter  $[-\infty, -0.5]$  and  $[0.5, +\infty]$  filtered out. We extract the yaw parameter using DECA. We call these the *Negative Yaw Filtered* (NYF) and *Positive Yaw Filtered* (PYF) datasets/networks, respectively. Both datasets have roughly the same number of samples: the *Negative Yaw Filtered* dataset has 440,448 training samples and the *Positive Yaw Filtered* dataset has 449,243 samples. We also train a *Normal* network on all of the 491,542 samples of the unfiltered CASIA WebFace dataset. We then test both the normal network and the yaw-weakened networks on simulated samples. We do this by generating two images of a same person, by fixing the shape, texture and expression parameters. The first image is a frontal image of the person. We vary the yaw component of the second image in the  $[-1, 1]$  range, where a  $-1$  and  $1$  in the yaw component indicate a fully-profile face on the negative and positive sides and plot the resulting cosine similarity computed between the embeddings of the two images. This cosine similarity should be large given that the two images presented are of the same identity. A low cosine similarity means that the network has less confidence that the images show the same person.

In Figure 2a, we observe that each yaw-weakened network makes less accurate predictions for images presenting high yaw in their respective weakness intervals. Note that all networks perform almost identically with frontal samples. Also, note that the normal network is almost always superior to the two weakened networks. This is a natural result of having 10% more training data. This plot is an average over 25 different identities that we obtain by grid-sampling the first texture and shape components over the range  $[-\sigma, \sigma]$ .

We compute the area between the curves for the  $[-1.0, -0.5]$ ,  $[-0.5, 0.5]$  and  $[0.5, 1.0]$  intervals. We observe in Table 1 (left) that in the  $[-1.0, -0.5]$  yaw range, precisely where the NYF network has been weakened, the area between the Normal-NYF curves is large and the area between the Normal-PYF curves is small. Conversely, in the  $[0.5, 1.0]$  range, where PYF has been weakened, we see that the difference between the Normal-PYF curves is large and the Normal-NYF difference is smaller. Also, we observe near identical differences between Normal-NYF and Normal-PYF

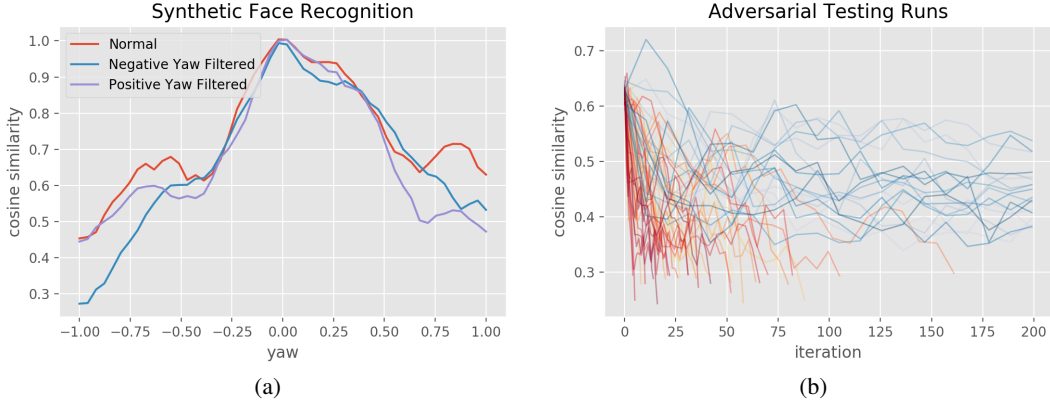


Figure 2: **(a)** Recognition cosine similarity between two simulated pairs of the same identity (averaged over 25 different identities). The first image is frontal and we vary the yaw of the second image. The *Negative Yaw Filtered* network exhibits less accurate predictions for highly negative yaw images than both the *Positive Yaw Filtered* and *Normal* networks. The *Positive Yaw Filtered* network exhibits less accurate predictions for highly positive yaw images than both the *Negative Yaw Filtered* and *Normal* networks. **(b)** A set of adversarial testing runs. Yellow-Red curves denote successful runs and Blue curves denote unsuccessful attempts. In most runs adversarial testing quickly locks onto specific weaknesses and produces adversarial examples in few iterations. For unsuccessful attempts, adversarial testing converges to local minima that are not below the threshold.

Table 1: Quantitative differences between evaluation of the purposefully weakened *Negative Yaw Filtered* (NYF) and *Positive Yaw Filtered* (PYF) and the *Normal* on synthetic faces (bold values for emphasis). Blue values in the table on the right mean the differences are statistically significant with  $p < 0.01$ .

↓ Models / Yaw Interval →	Area Between Curves			↓ Models / Yaw →	Mean Difference		
	[-1.0, -0.5]	[-0.5, 0.5]	[0.5, 1.0]		-1.0	0.0	1.0
Normal:NYF	<b>8.69</b>	2.83	4.68	Normal-NYF	0.18	0.01	0.10
Normal:PYF	2.71	2.76	<b>8.46</b>	Normal-PYF	0.01	0.00	0.16
				NYF-PYF	-0.17	-0.01	0.06

in the  $[-0.5, 0.5]$ , which is a consequence of the lesser amount of training data of NYF and PYF networks. We also compute pairwise mean differences for the different populations of Normal, NYF and PYF networks and present them in Table 1 (right). We highlight in blue the statistically significant differences. We have similar results as in Table 1 (left).

This evidence indicates that when a weakness is purposefully created in a network by filtering out key samples in the real training dataset, we can retrieve this weakness using our face simulator. This gives credence to the idea that we are able to find simulated adversarial examples in the semantic image manifold that will give us knowledge about adversarial examples in the real world.

#### 4.4 Simulated Adversarial Testing of Face Recognition Models

In this section we evaluate adversarial testing of face recognition models in the face verification scenario. Specifically, we generate samples using the FLAME face model and our proposed search algorithm that fool the face recognition model.

We train a CBAM-ResNet50 on CASIA WebFace for 20 epochs. This network achieves a 99.1% accuracy on the LFW test set for the face verification task. The evaluation task is face verification between two synthetic images of a same person’s face, one frontal and one profile image. We vary the first 15 shape parameters as well as the first 15 texture parameters for our generated identities, ranging from  $-2\sigma$  and  $2\sigma$  where  $\sigma$  is the standard deviation of each parameter in question.

Table 2: CBAM-ResNet50 face verification accuracy over synthetic datasets generated by random sampling or by adversarial testing (Adv. Testing).

Method	Accuracy ↓	Avg. Cosine Similarity ↓
Random Sampling	99%	0.518
Adv. Testing	36.5%	0.263

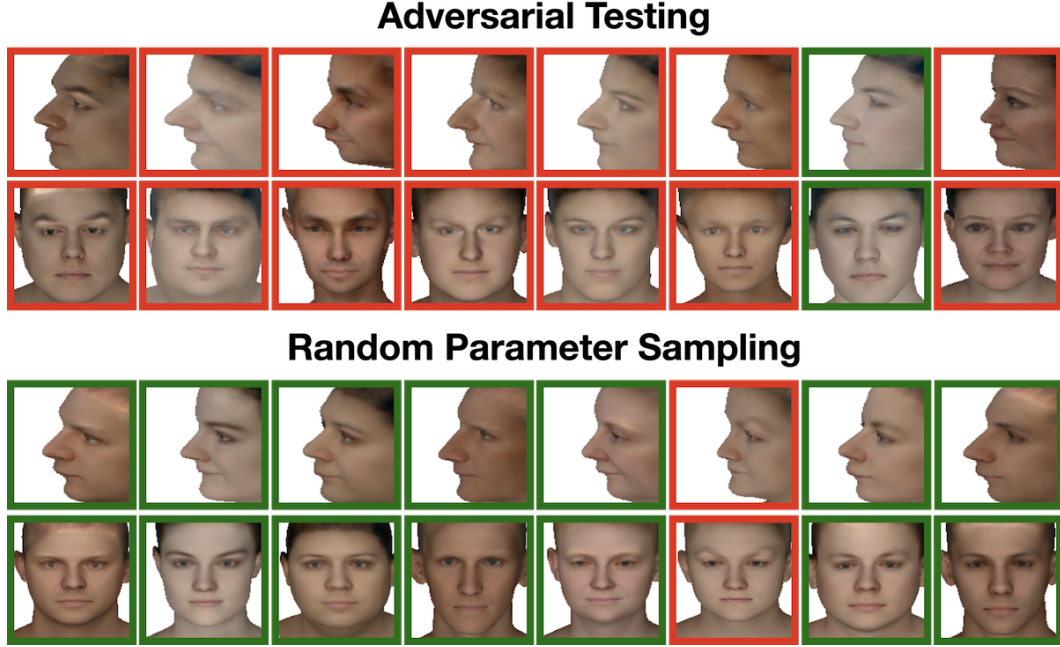


Figure 3: Face models obtained using adversarial testing (above) and random parameter sampling (below). The border line colors denote whether the face recognition network can successfully verify the pairs, with red denoting a failed verification and green denoting a successful verification. We obtain adversarial samples using our adversarial testing method more consistently than with random parameter sampling. Some recurring features of adversarial faces are ambiguous frontal/profile features (e.g. long nose, tucked jaw), pale/dark skin colors and left/right asymmetries.

We propose testing the network using 100 identities obtained by uniformly sampling these parameters. We also test the network using 100 runs of our adversarial testing algorithm (200 maximum iterations). In Table 2, we show that the random sampling testing regime achieves an accuracy of 99%, which is very close to the 99.1% real-world accuracy of the network on the LFW test set. Using adversarial testing, the network exhibits an accuracy of 36.5%, which is a marked drop in verification performance. We also compute the average cosine similarity between pairs, showing that adversarial testing generates highly adversarial samples (success threshold  $T = 0.298$ ) whereas random samples are highly non-adversarial on average. In Figure 3 we show a subset of the generated samples for both the adversarial testing (above) and random sampling (below). In Figure 2b we show the cosine similarity curves for a random subset of the adversarial testing runs, showing both the attempts that produce adversarial examples in few iterations and unsuccessful attempts that converge to local minima without becoming adversarial.

#### 4.5 Finding Adversarial Regions of Face Recognition Models

We use our method described in Algorithm 2 to find adversarial regions in simulation for face recognition models. We do this in the face verification scenario between a frontal image with neutral expression and a profile image with an open jaw. We vary the first shape and texture parameters to find an adversarial sample, and then find the connected components to those seed parameters. We also grid sample both parameters in order to plot the synthetic sample surface. We show the surface



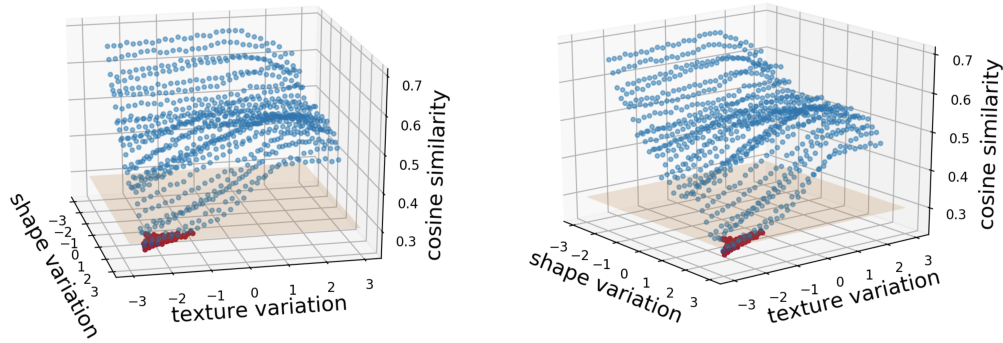


Figure 4: Our algorithm finds the adversarial region (red) in the shape-texture landscape (blue). We also plot the adversarial threshold plane (orange).

of all synthetic samples (blue), along with the adversarial region (red) and the adversarial threshold plane (orange) in Figure 4.

## 5 Related Work

Testing computer vision models on synthetic data is not a new idea [33, 28, 19, 21, 22, 37], although there is a relative paucity of work in this area. More common are investigations on training models on synthetic data [11, 35, 34, 8]. Recent works even learn to adapt the generative distribution of synthetic data in order for the model to learn better representations [36, 26, 12, 3, 20, 2] or adapt the pixels or features of the synthetic data to bridge the synthetic-to-real domain gap [13, 7, 43, 42, 17, 32]. In contrast to this body of work, we propose to search the parameter space of a simulator in order to test the model in an adversarial manner. There is very interesting work that adapts generative distributions in order to test models [1, 49, 39]. In contrast to [49, 39] we test computer vision models that are trained on real data, which is a more challenging scenario since the domain shift problem has to be described and overcome. Different from [49, 1, 39] we work on the domain of face recognition instead of object classification or VQA, where we have a higher number of simulator parameters including shape, expression, texture, lighting and pose parameters. We search the parameter landscape using a continuous policy that explores all parameters simultaneously, which is important since model performance does not vary independently with each parameter (as Figure 4 shows), and discrete changes in parameter space can yield high loss changes due to gradient sharpness. A final difference with these and work on traditional adversarial attacks [41, 30, 6, 15, 27] is that we present a method that not only finds one isolated adversarial latent vector, but locates regions of them.

## 6 Conclusion

In this work we propose to test machine learning models by searching for semantically realistic adversarial examples using a simulator. We present a framework for simulated adversarial testing, as well as a method to find simulated adversarial examples. Finally, we present a method to find connected regions of adversarial examples in the semantic space of latent variables and we evaluate our methods on contemporary face recognition networks using a face simulator.

We find that face recognition networks that have real world weaknesses due to biased training sets with respect to pose can be analyzed using controllable simulated faces and these weaknesses can be discerned. We also find that contemporary face recognition networks are fooled by specific combinations of simulated face shapes and textures. Some recurring features of adversarial faces are ambiguous frontal/profile features (e.g. long nose, tucked jaw), pale/dark skin colors and left/right asymmetries. When such a network is tested using adversarial testing, its accuracy plummets compared to random testing or testing on a real-world test set such as LFW. We show evidence that these adversarial examples are not isolated, but part of connected components of adversarial examples in the manifold of semantically plausible images.

**Broader impact.** The plausible negative social consequences of this work are tightly linked with overall negative consequences of facial analysis systems. An approach that improves testing for face recognition systems such as the one we propose can be used to improve recognition rates on minorities, persecuted groups and oppressed individuals. This is a larger problem acting on any work that can potentially impact facial analysis, and we argue that our work has an asymmetric potential for applications that have a positive social impact. Given that researchers have proven that there exists gender and racial bias of beneficial face analysis systems [5, 14, 16], by better testing such systems these biases can be diagnosed and mitigated, meaning that minorities can more readily benefit from these technologies.

## References

- [1] M. A. Alcorn, Q. Li, Z. Gong, C. Wang, L. Mai, W.-S. Ku, and A. Nguyen. Strike (with) a pose: Neural networks are easily fooled by strange poses of familiar objects. In *Proceedings of the IEEE/CVF Conference on Computer Vision and Pattern Recognition*, pages 4845–4854, 2019.
- [2] O. M. Andrychowicz, B. Baker, M. Chociej, R. Jozefowicz, B. McGrew, J. Pachocki, A. Petron, M. Plappert, G. Powell, A. Ray, et al. Learning dexterous in-hand manipulation. *The International Journal of Robotics Research*, 39(1):3–20, 2020.
- [3] S. Beery, Y. Liu, D. Morris, J. Piavis, A. Kapoor, N. Joshi, M. Meister, and P. Perona. Synthetic examples improve generalization for rare classes. In *Proceedings of the IEEE/CVF Winter Conference on Applications of Computer Vision (WACV)*, March 2020.
- [4] S. Ben-David, J. Blitzer, K. Crammer, A. Kulesza, F. Pereira, and J. W. Vaughan. A theory of learning from different domains. *Machine learning*, 79(1):151–175, 2010.
- [5] J. Buolamwini and T. Gebru. Gender shades: Intersectional accuracy disparities in commercial gender classification. In *Conference on fairness, accountability and transparency*, pages 77–91, 2018.
- [6] N. Carlini and D. Wagner. Towards evaluating the robustness of neural networks. In *2017 IEEE Symposium on Security and Privacy (SP)*, pages 39–57. IEEE, 2017.
- [7] Y.-H. Chen, W.-Y. Chen, Y.-T. Chen, B.-C. Tsai, Y.-C. Frank Wang, and M. Sun. No more discrimination: Cross city adaptation of road scene segmenters. In *The IEEE International Conference on Computer Vision (ICCV)*, Oct 2017.
- [8] A. Dosovitskiy, G. Ros, F. Codevilla, A. Lopez, and V. Koltun. Carla: An open urban driving simulator. In *Conference on robot learning*, pages 1–16. PMLR, 2017.
- [9] Y. Feng, H. Feng, M. J. Black, and T. Bolkart. Learning an animatable detailed 3D face model from in-the-wild images. *ACM Transactions on Graphics (ToG), Proc. SIGGRAPH*, 40(4):88:1–88:13, Aug. 2021.
- [10] G. Gafni, J. Thies, M. Zollhöfer, and M. Nießner. Dynamic neural radiance fields for monocular 4d facial avatar reconstruction. *arXiv preprint arXiv:2012.03065*, 2020.
- [11] A. Gaidon, Q. Wang, Y. Cabon, and E. Vig. Virtual worlds as proxy for multi-object tracking analysis. In *Proceedings of the IEEE conference on computer vision and pattern recognition*, pages 4340–4349, 2016.
- [12] Y. Ganin, T. Kulkarni, I. Babuschkin, S. M. A. Eslami, and O. Vinyals. Synthesizing programs for images using reinforced adversarial learning. In *ICML*, 2018.
- [13] Y. Ganin, E. Ustinova, H. Ajakan, P. Germain, H. Larochelle, F. Laviolette, M. Marchand, and V. Lempitsky. Domain-adversarial training of neural networks. *J. Mach. Learn. Res.*, 17(1):2096–2030, Jan. 2016.
- [14] R. V. Garcia, L. Wandzik, L. Grabner, and J. Krueger. The harms of demographic bias in deep face recognition research. In *2019 International Conference on Biometrics (ICB)*, pages 1–6, 2019.

- [15] I. Goodfellow, J. Shlens, and C. Szegedy. Explaining and harnessing adversarial examples. In *Proc. ICLR*, 2015.
- [16] P. Grother, M. Ngan, and K. Hanaoka. Face recognition vendor test part 3: Demographic effects, 2019-12-19 2019.
- [17] J. Hoffman, E. Tzeng, T. Park, J.-Y. Zhu, P. Isola, K. Saenko, A. Efros, and T. Darrell. Cycada: Cycle-consistent adversarial domain adaptation. In *International conference on machine learning*, pages 1989–1998. PMLR, 2018.
- [18] G. B. Huang, M. Ramesh, T. Berg, and E. Learned-Miller. Labeled faces in the wild: A database for studying face recognition in unconstrained environments. Technical Report 07-49, University of Massachusetts, Amherst, October 2007.
- [19] J. Johnson, B. Hariharan, L. Van Der Maaten, L. Fei-Fei, C. Lawrence Zitnick, and R. Girshick. Clevr: A diagnostic dataset for compositional language and elementary visual reasoning. In *Proceedings of the IEEE Conference on Computer Vision and Pattern Recognition*, pages 2901–2910, 2017.
- [20] A. Kar, A. Prakash, M.-Y. Liu, E. Cameracci, J. Yuan, M. Rusiniak, D. Acuna, A. Torralba, and S. Fidler. Meta-sim: Learning to generate synthetic datasets. In *Proceedings of the IEEE/CVF International Conference on Computer Vision (ICCV)*, October 2019.
- [21] A. Kortylewski, B. Egger, A. Schneider, T. Gerig, A. Morel-Forster, and T. Vetter. Empirically analyzing the effect of dataset biases on deep face recognition systems. In *Proceedings of the IEEE Conference on Computer Vision and Pattern Recognition Workshops*, pages 2093–2102, 2018.
- [22] A. Kortylewski, B. Egger, A. Schneider, T. Gerig, A. Morel-Forster, and T. Vetter. Analyzing and reducing the damage of dataset bias to face recognition with synthetic data. In *Proceedings of the IEEE Conference on Computer Vision and Pattern Recognition Workshops*, pages 2261–2268, 2019.
- [23] T. Li, T. Bolkart, M. J. Black, H. Li, and J. Romero. Learning a model of facial shape and expression from 4D scans. *ACM Transactions on Graphics, (Proc. SIGGRAPH Asia)*, 36(6):194:1–194:17, 2017.
- [24] T. Li, M. Slavcheva, M. Zollhoefer, S. Green, C. Lassner, C. Kim, T. Schmidt, S. Lovegrove, M. Goesele, and Z. Lv. Neural 3d video synthesis. *arXiv preprint arXiv:2103.02597*, 2021.
- [25] H. Lieberman. How to color in a coloring book. *SIGGRAPH Comput. Graph.*, 12(3):111–116, Aug. 1978.
- [26] G. Louppe and K. Cranmer. Adversarial variational optimization of non-differentiable simulators. *arXiv preprint arXiv:1707.07113*, 2017.
- [27] A. Madry, A. Makelov, L. Schmidt, D. Tsipras, and A. Vladu. Towards deep learning models resistant to adversarial attacks. In *International Conference on Learning Representations*, 2018.
- [28] N. Mayer, E. Ilg, P. Hausser, P. Fischer, D. Cremers, A. Dosovitskiy, and T. Brox. A large dataset to train convolutional networks for disparity, optical flow, and scene flow estimation. In *Proceedings of the IEEE conference on computer vision and pattern recognition*, pages 4040–4048, 2016.
- [29] B. Mildenhall, P. P. Srinivasan, M. Tancik, J. T. Barron, R. Ramamoorthi, and R. Ng. Nerf: Representing scenes as neural radiance fields for view synthesis. In *European Conference on Computer Vision*, pages 405–421. Springer, 2020.
- [30] N. Papernot, P. McDaniel, I. Goodfellow, S. Jha, Z. B. Celik, and A. Swami. Practical black-box attacks against machine learning. In *Proceedings of the 2017 ACM on Asia conference on computer and communications security*, pages 506–519. ACM, 2017.
- [31] P. Paysan, R. Knothe, B. Amberg, S. Romdhani, and T. Vetter. A 3d face model for pose and illumination invariant face recognition. In *2009 sixth IEEE international conference on advanced video and signal based surveillance*, pages 296–301. Ieee, 2009.

- [32] X. Peng, Q. Bai, X. Xia, Z. Huang, K. Saenko, and B. Wang. Moment matching for multi-source domain adaptation. In *Proceedings of the IEEE/CVF International Conference on Computer Vision*, pages 1406–1415, 2019.
- [33] N. Pinto, J. J. DiCarlo, and D. D. Cox. Establishing good benchmarks and baselines for face recognition. In *Workshop on Faces In ‘Real-Life’ Images: Detection, Alignment, and Recognition*, 2008.
- [34] S. R. Richter, V. Vineet, S. Roth, and V. Koltun. Playing for data: Ground truth from computer games. In *European Conference on Computer Vision*, pages 102–118. Springer, 2016.
- [35] G. Ros, L. Sellart, J. Materzynska, D. Vazquez, and A. M. Lopez. The synthia dataset: A large collection of synthetic images for semantic segmentation of urban scenes. In *Proceedings of the IEEE conference on computer vision and pattern recognition*, pages 3234–3243, 2016.
- [36] N. Ruiz, S. Schuler, and M. Chandraker. Learning to simulate. In *International Conference on Learning Representations*, 2018.
- [37] N. Ruiz, B.-J. Theobald, A. Ranjan, A. H. Abdelaziz, and N. Apostoloff. Morphnet: One-shot face synthesis gan for detecting recognition bias. *arXiv preprint arXiv:2012.05225*, 2020.
- [38] H. Salman, A. Ilyas, L. Engstrom, S. Vemprala, A. Madry, and A. Kapoor. Unadversarial examples: Designing objects for robust vision. *arXiv preprint arXiv:2012.12235*, 2020.
- [39] M. Shu, C. Liu, W. Qiu, and A. Yuille. Identifying model weakness with adversarial examiner. In *Proceedings of the AAAI Conference on Artificial Intelligence*, volume 34, pages 11998–12006, 2020.
- [40] A. R. Smith. Tint fill. *SIGGRAPH Comput. Graph.*, 13(2):276–283, Aug. 1979.
- [41] C. Szegedy, W. Zaremba, I. Sutskever, J. Bruna, D. Erhan, I. Goodfellow, and R. Fergus. Intriguing properties of neural networks. In *In Proc. ICLR*, 2014.
- [42] Y.-H. Tsai, W.-C. Hung, S. Schuler, K. Sohn, M.-H. Yang, and M. Chandraker. Learning to adapt structured output space for semantic segmentation. In *The IEEE Conference on Computer Vision and Pattern Recognition (CVPR)*, June 2018.
- [43] E. Tzeng, J. Hoffman, K. Saenko, and T. Darrell. Adversarial discriminative domain adaptation. In *Proceedings of the IEEE conference on computer vision and pattern recognition*, pages 7167–7176, 2017.
- [44] H. Wang, Y. Wang, Z. Zhou, X. Ji, D. Gong, J. Zhou, Z. Li, and W. Liu. Cosface: Large margin cosine loss for deep face recognition. In *Proceedings of the IEEE conference on computer vision and pattern recognition*, pages 5265–5274, 2018.
- [45] R. J. Williams. Simple statistical gradient-following algorithms for connectionist reinforcement learning. *Machine learning*, 8(3-4):229–256, 1992.
- [46] S. Woo, J. Park, J.-Y. Lee, and I. S. Kweon. Cbam: Convolutional block attention module. In *Proceedings of the European conference on computer vision (ECCV)*, pages 3–19, 2018.
- [47] D. Yi, Z. Lei, S. Liao, and S. Z. Li. Learning face representation from scratch. *arXiv preprint arXiv:1411.7923*, 2014.
- [48] A. L. Yuille and C. Liu. Deep nets: What have they ever done for vision? *International Journal of Computer Vision*, 129(3):781–802, 2021.
- [49] X. Zeng, C. Liu, Y.-S. Wang, W. Qiu, L. Xie, Y.-W. Tai, C.-K. Tang, and A. L. Yuille. Adversarial attacks beyond the image space. In *Proceedings of the IEEE/CVF Conference on Computer Vision and Pattern Recognition*, pages 4302–4311, 2019.

## A. Appendix

We perform further simulated adversarial testing experiments on a CBAM-ResNet50 trained on CASIA WebFace for 20 epochs. This network achieves a 99.1% accuracy on the LFW test set. The evaluation task is face verification between two synthetic images of a same person’s face, one frontal and one profile image. We vary the first 30 shape parameters as well as the first 30 texture parameters for our generated identities, ranging from  $-2\sigma$  and  $2\sigma$  where  $\sigma$  is the standard deviation of each parameter in question. We also vary the yaw pose parameter within  $[-1, +1]$ , corresponding to variations of  $[-\pi/2, +\pi/2]$  degrees and the pitch pose parameter from  $[-1/4, +1/4]$  corresponding to variations within  $[-\pi/8, +\pi/8]$ . Thus, in this case our algorithm has to learn 62 parameters. This is a more challenging scenario due to the larger dimensionality of the policy output.

We perform 100 runs of our adversarial testing algorithm (200 maximum iterations). We also perform 1,000 iterations of uniform random sampling of parameters. We compare the two in Table 3 and we show that the face recognition network achieves an accuracy of 99.9% on the random sample regime, also close to the 99.1% real-world accuracy of the network on the LFW test set. Using adversarial testing, the network exhibits an accuracy of 49%, a marked drop in verification performance. We also compute the average cosine similarity between pairs, showing that adversarial testing generates highly adversarial samples (success threshold  $T = 0.298$ ) whereas random samples are highly non-adversarial on average. Further, adversarial testing achieves 51 adversarial samples over 12,587 iterations while random sampling achieves only one adversarial sample over 1,000 iterations. This makes adversarial testing 400% more sample efficient than random sampling in this specific scenario. In some of our tested scenarios and depending on the number of iterations, random sampling was not able to find any adversarial samples. We present an illustration in Figure 5, where a successful adversarial testing run is able to quickly lock onto a specific model weakness and produces an adversarial example in tens of iterations while random sampling takes more than 600 iterations to produce one. We can also see that the average cosine similarity of randomly sampled pairs is highly non-adversarial (0.766). In Figure 6, we show several successful adversarial testing runs (orange/red) and a random sampling run. We see the same principle of quick generation of adversarial samples exemplified here. Unsuccessful attempts usually converge to a low cosine similarity without becoming adversarial and remain in the high-dimensional local minima. Finally, we show an example of our adversarial testing method in action where all 30 shape, 30 texture and 2 pose parameters are being learned jointly in Figure 7. The algorithm finds an adversarial sample that reveals model weaknesses such as vulnerability to unusual poses, exaggerated facial features and distinct skin color.

**Illustration of Learning on 2D Surface** We use our method to find adversarial regions in simulation for face recognition models. We do this in the face verification scenario between a frontal image with neutral expression and a profile image with an open jaw. We vary the first shape and texture parameters to find an adversarial sample, and then find the connected components to those seed parameters. We also grid sample both parameters in order to plot the synthetic sample surface. We show the surface of all synthetic samples (blue), along with the adversarial region (red) and the adversarial threshold plane (orange) in Figure 8. Additionally, here we show the learning trajectory (lighter red) of the initial phase of our algorithm that finds the seed adversarial parameters to subsequently find the adversarial parameter region. Our method starts at the  $(0, 0)$  shape and texture coordinate and explores the landscape to quickly find simulator parameters that generate faces that are adversarial for the face recognition model.

## Acknowledgements

We thank Romain Lopez for the interesting conversations and suggestions.

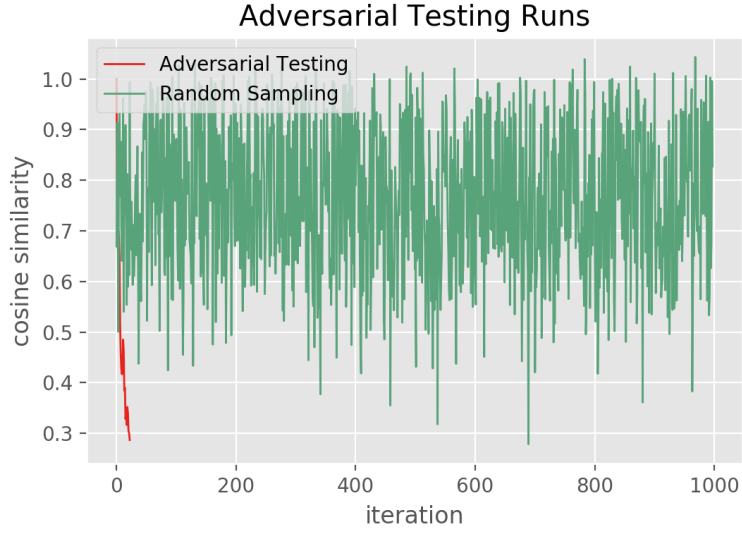


Figure 5: Evolution of cosine similarity for adversarial testing and random parameter sampling. Most runs of adversarial testing quickly lock onto specific weaknesses and produce adversarial examples in few iterations while random parameter sampling averages highly non-adversarial examples.

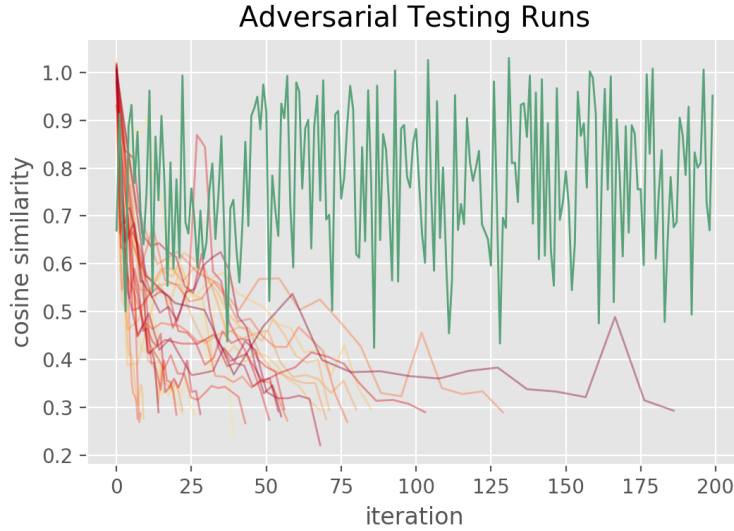


Figure 6: Evolution of cosine similarity for successful adversarial testing runs and random parameter sampling. Runs of adversarial testing quickly lock onto specific weaknesses and produce adversarial examples in few iterations while random parameter sampling averages highly non-adversarial examples.

Table 3: CBAM-ResNet50 face verification accuracy over synthetic datasets generated by random sampling or by adversarial testing (Adv. Testing). We vary 30 shape parameters, 30 texture parameters and the yaw and pitch pose parameters.

Method	Accuracy ↓	Avg. Cosine Similarity ↓
Random Sampling	99.9%	0.766
Adv. Testing	49%	0.282



Figure 7: A sequence of generated synthetic samples undergoing adversarial testing (left to right, top to bottom). Our method searches through all 30 shape, 30 texture and 2 pose parameters jointly to find an adversarial face. The border line colors denote whether the face recognition network can successfully verify the pairs, with red denoting a failed verification and green denoting a successful verification.

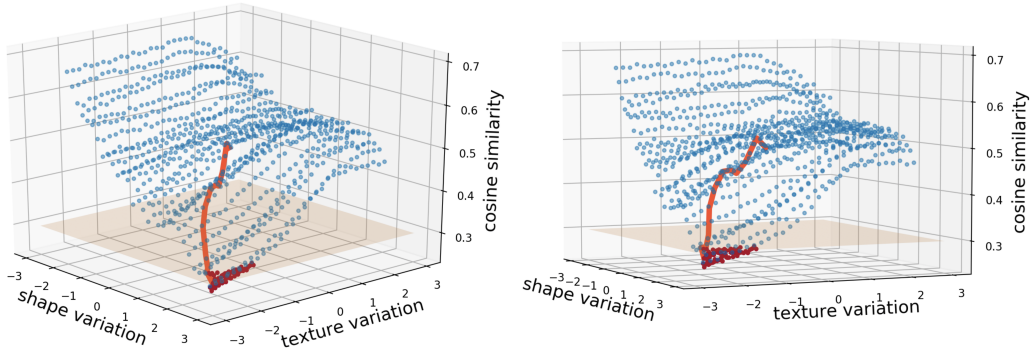


Figure 8: Our algorithm finds the adversarial region (red) in the shape-texture landscape (blue). We also plot the initial learning trajectory of our algorithm in lighter red that yields the seed adversarial simulator parameters. We also plot the adversarial threshold plane (orange).